Magnetic upconverting fluorescent $NaGdF_4:Ln^{3+}$ and iron-oxide@$NaGdF_4:Ln^{3+}$ nanoparticles

Navadeep Shrivastava,[1] Uéslen Rocha,[2] Diego Muraca,[3] Carlos Jacinto,[2] Sergio Moreno,[4] J. M. Vargas,[4] and S. K. Sharma[1,a]
[1]*Department of Physics, Federal University of Maranhão, Sao Luis 65080-805, MA, Brazil*
[2]*Institute of Physics, Federal University of Alagoas, Maceió 57480-000, AL, Brazil*
[3]*Institute of Physics, State University of Campinas, Campinas 13083-859, SP, Brazil*
[4]*Centro Atomico Bariloche, CONICET, S. C. de Bariloche, 8400 Rio Negro, Bariloche, Argentina*

(Presented 8 November 2017; received 2 October 2017; accepted 1 November 2017; published online 19 December 2017)

Microwave assisted solvothermal method has been employed to synthesize multifunctional upconverting β-$NaGdF_4:Ln^{3+}$ and magnetic-upconverting Fe_3O_4/γ-Fe_2O_3@$NaGdF_4:Ln^{3+}$ (Ln = Yb and Er) nanoparticles. The powder x-ray diffraction data confirms the hexagonal structure of $NaGdF_4:Ln^{3+}$ and high resolution transmission electron microscopy shows the formation of rod shaped $NaGdF_4:Ln^{3+}$ (~ 20 nm) and ovoid shaped Fe_3O_4/γ-Fe_2O_3@$NaGdF_4:Ln^{3+}$ (~ 15 nm) nanoparticles. The magnetic hysteresis at 300 K for β-$NaGdF_4:Ln^{3+}$ demonstrates paramagnetic features, whereas iron-oxide@β-$NaGdF_4:Ln^{3+}$ exhibits superparamagnetic behavior along with a linear component at large applied field due to paramagnetic $NaGdF_4$ matrix. Both nanoparticle samples provide an excellent green emitting [($^2H_{11/2}$, $^4S_{3/2}$)→$^4I_{15/2}$ (~ 540 nm)] upconversion luminescence emission under excitation at 980 nm. The energy migration between Yb and Er in $NaGdF_4$ matrix has been explored from 300-800 nm. Intensity variation of blue, green and red lines and the observed luminescence quenching due to the presence of Fe_3O_4/γ-Fe_2O_3 in the composite has been proposed. These kinds of materials contain magnetic and luminescence characteristics into single nanoparticle open new possibility for bioimaging applications. https://doi.org/10.1063/1.5007748

INTRODUCTION

For the last two decades, scientific and industrial interest in developing materials has culminated multiple times especially in the preparation of quality materials with enhanced multifunctionality at nanoscale.[1–4] For instance, the nanocomposites containing luminescent and magnetic characteristics are trending in a wide range of applications, such as bioimaging, diagnostic, and therapeutics. Meanwhile, magnetic iron oxide nanoparticles have also been proved promising hence allowed in a wide range of biomedical applications.[2,4] However, a small application oriented work has been performed combining iron oxide with luminescent materials due to the so called quenching effect induced by semimetallic Fe_3O_4 during simultaneous optical excitation/emission with applied external magnetic field.[5–7] These multifunctional nanoparticles can serve as luminescent markers; they can also be controlled by an external magnetic field.[8] Several parameters such as magnetic, electrostatic, hydrophobic and many chemical interaction creates a boundary and limitation for the real application of multifunctional nanoparticles as these issues generates low chemical stability and aggregation at nanoscale.[2,9,10] To resolve above mentioned quenching issue, aggregation, and agglomeration etc., few approaches are in use such as: a magnetic core coated with silica, polymer or lipid containing

[a]surender76@gmail.com

fluorescent components; covalently bounded to a fluorophore via a spacer; a fluorescent shell; and/or quantum dots encapsulated in a polymer or silica matrix.

Lanthanide (Ln^{3+}) doped rare earth fluoride upconversion (UC) nanoparticles absorb near–infrared (NIR) photons and emit higher energy photons, either in the ultraviolet–visible-NIR regions and are being potentially used in industry and biomedical applications.[11,12] They are preferred nano-luminescent materials because of high penetration depth and signal–to–noise ratio, a large anti-Stokes shift, a long luminescence lifetime, good chemical and photochemical stability, resistance to photo bleaching, low auto–fluorescence and excellent detection sensitivity. Additionally, Gd^{3+} containing UC nanoparticles exhibit paramagnetism at room temperature and they can efficiently alter the spin–spin relaxation time of surrounding water protons because Gd possesses seven unpaired electrons.[13] Therefore, Gd^{3+} containing rare earth fluoride UC luminescence nanomaterials have been developed as potential T1–weighted MR imaging contrast agents in biomedical applications and are being explored.[5,14]

In this article, we present a facile microwave solvothermal method for the synthesis of bifunctional β-$NaGdF_4$:Ln^{3+} nanoparticles and direct coating of the same over surface of iron-oxide core nanoparticles. We focus on the changes of the intensity of emission peaks with lifetime variation in these two bifunctional nanomaterials and provide direct evidence of quenching induced by magnetite/maghemite phase. The nanocomposite particles have been thoroughly characterized using XRD, HRTEM, photoluminescence and dc magnetization measurements. These investigating techniques suggest a comparative approach to understand two different templates of magnetic-luminescent nanoparticles.

EXPERIMENTAL SECTION

Synthesis of iron-oxide@$NaGdF_4$:Ln^{3+}

The iron-oxide nanoparticles were prepared using method described in Ref. 15. A facile microwave assisted solvothermal reaction has been proposed for the synthesis of NaGdF4:$Ln3^{+}$ and iron-oxide@$NaGdF_4$:Ln^{3+} (Ln^{3+} = 20%Yb, 2% Er) nanoparticles. The shell $NaGdF_4$:Ln^{3+} was prepared in following way: firstly, 0.78 mmol $GdCl_3.6H_2O$, 0.20 mmol $YbCl_3.6H_2O$ and 0.02 mmol $ErCl_3.6H_2O$ was added into solution containing 16 mL oleic acid to form rare earth oleate and 8 mL of 1-octadecene under continuous stirring at ambient temperature for 20 minutes. Meanwhile, 2.5 mmol NaOH was dissolved in 10 mL methanol and then 8 mL oleic acid was added by stirring to prepare Na-oleate translucent solution. The above two solutions were mixed quickly and stirred for additional 5 minutes. A separate solution of iron oxide nanoseeds prepared in 1-octadecene was poured in above solution slowly and stirred for 10 minutes at room temperature. Another solution of 4 mmol fluoride source (NH_4F) in 15 mL methanol was mixed properly in above solution. The mixture was transferred into the reaction vessel of a commercial microwave reactor working at 1000 W. The working cycle of the microwave reactor was set as (i) 20^0C/minute rapid heating until 150^0C from room temperature; and (ii) 40 minute at 150^0C. The system was allowed to cool quickly to room temperature and obtained samples were washed sequentially with methanol and ethanol, and then dried in an air oven at 50°C for 6 hours.

Instrumentation

The phase purities of all the samples were checked by using X-ray diffraction (XRD) measurements on a Brucker`s D8 Advance diffractometer using Cu K_α radiation (λ= 1.54 A°). The size and shape morphology were characterized using transmission electron microscopy (TEM, FEI Tecnai, 200 keV). The MPMS3 Quantum Design SQUID magnetometer was used for the dc magnetic measurement, whereas a spectrophotometer (Horiba NanoLog spectrofluorimeter) equipped with an external excitation laser source of 980 nm was used for the upconversion experiments.

RESULTS AND DISCUSSION

The phase structure of synthesized iron-oxide, $NaGdF_4$:Ln^{3+} and iron-oxide@$NaGdF_4$:Ln^{3+} nanoparticles were determined by XRD patterns (Figure 1). The XRD pattern of iron-oxide was

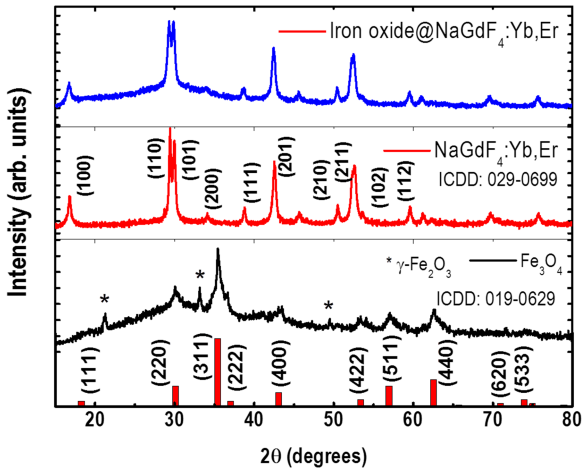

FIG. 1. X-ray powder diffraction patterns of cubic Fe_3O_4/γ-Fe_2O_3, hexagonal $NaGdF_4$:Yb, Er and Fe_3O_4/γ-Fe_2O_3@$NaGdF_4$:Yb, Er nanoparticles.

indexed to the face-centered cubic Fe_3O_4 spinel structure (Fd3m space-group) (ICDD#019-0629). Moreover, the as-prepared Fe_3O_4 was partially reduced into γ-Fe_2O_3 phase (ICDD#039-1346) (highlighted by star in Figure 1). Furthermore, by comparing with the ICDD#027-0699, the XRD pattern for $NaGdF_4$:Yb,Er nanoparticles has been indexed for hexagonal structure with space group $P\bar{6}$ For iron-oxide@$NaGdF_4$:Ln^{3+} nanocomposites, besides the characteristic diffractions of Fe_3O_4/γ-Fe_2O_3, the obvious diffraction peaks were indexed to $NaGdF_4$:Ln^{3+} (ICDD#027-0699). The weakening of the Fe_3O_4/γ-Fe_2O_3, diffraction peaks in the nanocomposites indicates that the structure of Fe_3O_4/γ-Fe_2O_3@$NaGdF_4$:Ln^{3+} was formed successfully, although, lattice energy mismatch between iron oxide and $NaGdF_4$:Yb, Er suggest the formation of composite type structure.[8] The crystallite size was calculated by using Debye-Scherrer's equation[16,17] and the mean particle size of Fe_3O_4/γ-Fe_2O_3 nanoparticles was ~ 5 nm, whereas for $NaGdF_4$:Yb,Er, it was ~20 nm. After coating of $NaGdF_4$:Ln^{3+} on Fe_3O_4/γ-Fe_2O_3, the calculated size was ~ 15 nm, which is subsequently confirmed by particle size distribution obtained through TEM imaging (Figure 2).

Figure 2 shows the TEM images for Fe_3O_4/γ-Fe_2O_3, $NaGdF_4$:Ln^{3+}, and Fe_3O_4/γ-Fe_2O_3@$NaGdF_4$:Ln^{3+} nanoparticles. The spherical iron oxide nanoparticles of 5-6 nm were observed (Figure 2a). In Figure 2b, most of the particles have a rod like morphology and few particles appear to be close to a spherical shape. During coating process of iron-oxide with $NaGdF_4$:Yb, Er, the overall heterogeneous nucleation was slowed down and ovoid shaped morphology has been observed as shown in Figure 2c.

The green emitting visible UC luminescence spectra of $NaGdF_4$:Yb, Er and Fe_3O_4/γ-Fe_2O_3@$NaGdF_4$:Yb,Er nanoparticles have been shown in Figure 3a. On the basis of energy matching conditions the synthesized nanoparticles are discussed by observing the emission spectra (Figure 3, a & b). Under excitation at 980 nm, the green luminescence assigned to the ($^2H_{11/2}$, $^4S_{3/2}$)→$^4I_{15/2}$ (~ 540 nm) transition, red emission originating from the $^4F_{9/2}$→$^4I_{15/2}$ (~ 660 nm) transition and the blue emissions attributed to the $^4G_{11/2}$→$^4I_{15/2}$ (~ 378 nm), $^2H_{9/2}$→$^4I_{15/2}$ (~ 411 nm) transitions of Er^{3+} ions were observed. The overall green emission line intensity of Fe_3O_4/γ-Fe_2O_3@$NaGdF_4$:Yb, Er is approximately 30% of $NaGdF_4$:Yb, Er green line. Furthermore, the surface properties and crystallinity of $NaGdF_4$:Yb, Er nanoparticles can affect the different emitting levels of doped ions, and hence result in the different emission intensity of red, green and blue light and the ratio of these are also different in both samples. Hence, the reduction of intensities (green, blue and red) can be ascribed due to direct energy mismatch of cubic Fe_3O_4/γ-Fe_2O_3 and hexagonal $NaGdF_4$ matrix; reduction of radiative luminescence centers over the surface of luminescence shell of $NaGdF_4$:Ln^{3+} when iron-oxide provides a leakage path for radiative centers (Er^{3+}); and induced arrangement of magnetic domain ordering at the surface of iron oxide.

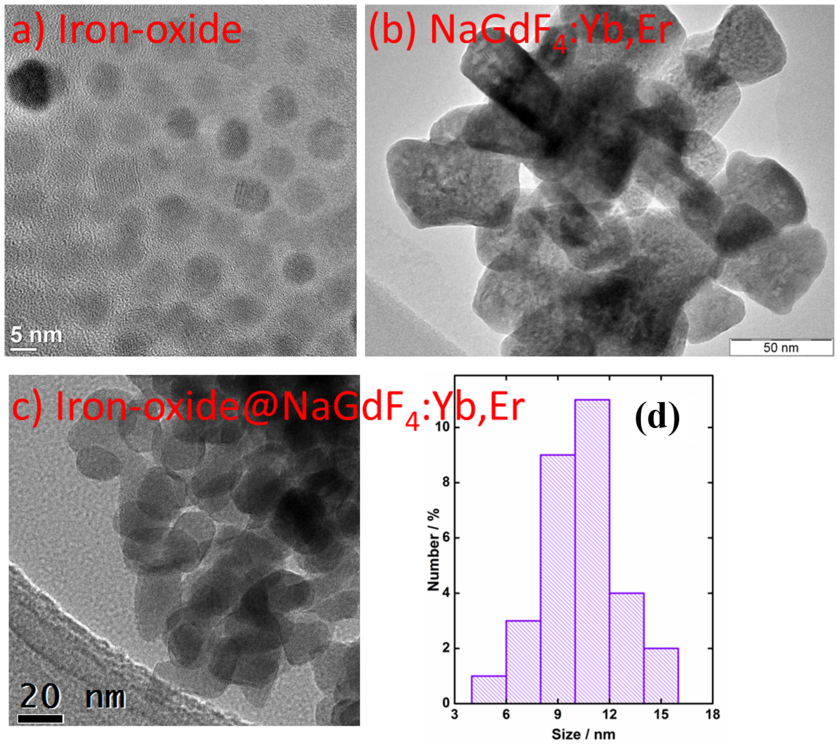

FIG. 2. High resolution transmission electron microscopy images of (a) spherical Fe_3O_4/γ-Fe_2O_3, (b) elongated rod like $NaGdF_4$: Yb, Er and (c) ovoid shaped Fe_3O_4/γ-Fe_2O_3@$NaGdF_4$:Yb, Er nanoparticles. (d) Particle Size distribution of Fe_3O_4/γ-Fe_2O_3@$NaGdF_4$:Yb,Er obtained by high resolution transmission electron microscopy.

The energy transfer (ET) in these samples can be explained in following steps under 980 nm of excitation: (i) Yb^{3+} ions are excited from the $^2F_{7/2}$ level to the $^2F_{5/2}$ level and then transfer their energies to the nearby Er^{3+} ions; (ii) the upper levels $^4G_{11/2}$, $^4F_{7/2}$, and $^4F_{9/2}$ of Er^{3+} ions are mainly

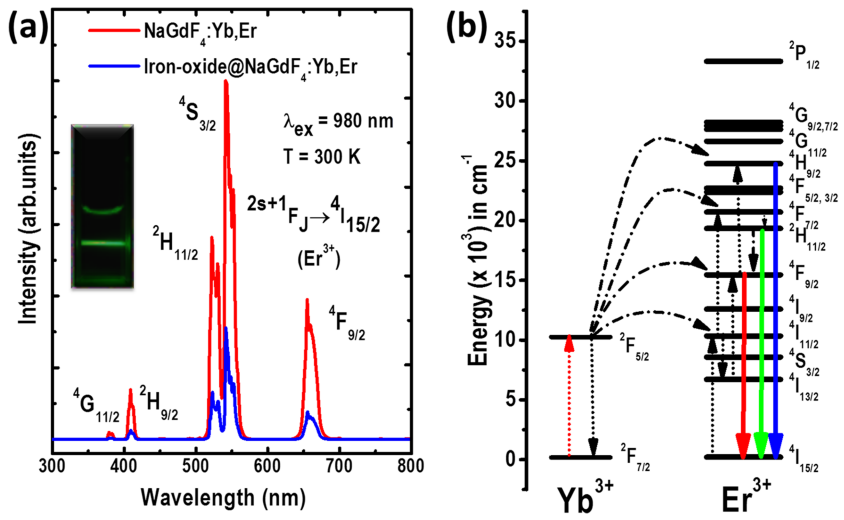

FIG. 3. (a) Upconverting luminescence (UCL) emission spectra of $NaGdF_4$:Yb,Er and Fe_3O_4/γ-Fe_2O_3@$NaGdF_4$:Yb,Er nanoparticles recorded in range from 300 nm to 800 nm, upon excitation of 980 laser. The inset figure shows the bright green emission for NPs dispersed in hexane at excitation of 980 nm. (b) Proposed energy transfer mechanism of photons in between Yb^{3+} and Er^{3+} ions doped in $NaGdF_4$ matrix.

populated by the ETs between Yb^{3+} and Er^{3+} ($^2F_{5/2}\rightarrow{}^2F_{7/2}$ (Yb); $^4I_{15/2}\rightarrow{}^4I_{11/2}$ (Er), $^4I_{13/2}\rightarrow{}^4F_{9/2}$ (Er), and $^4I_{11/2}\rightarrow{}^4F_{7/2}$ (Er)), (iii) the excited state absorption of the pump radiation from the $^4I_{11/2}$ and $^4I_{13/2}$ levels, and (iv) the cross relaxation between Er^{3+} ions, as depicted in Figure 3b.

The magnetic hysteresis loops recorded at 300 K for Fe_3O_4/γ-Fe_2O_3, $NaGdF_4$:Yb, Er and Fe_3O_4/γ-Fe_2O_3@$NaGdF_4$:Yb, Er nanoparticles are shown in Figure 4. $NaGdF_4$:Yb, Er nanoparticles were found paramagnetic with a susceptibilities of 0.8 x 10^{-2} of emu $g^{-1}Oe^{-1}$, whereas Fe_3O_4/γ-Fe_2O_3, and Fe_3O_4/γ-Fe_2O_3@$NaGdF_4$:Yb, Er clearly showed superparamagnetic behavior with negligible coercive field. The saturation magnetization (M_s) values were found to be 30.4 emu g^{-1} and 7.8 emu g^{-1} for Fe_3O_4/γ-Fe_2O_3 and Fe_3O_4/γ-Fe_2O_3@$NaGdF_4$:Yb, Er, respectively. These reductions in M_S were attributed to the variance in particle size distribution, prolonged existence relaxation of nanostructures and non-collinear spin arrangement/disorder spin on the surface of very small nanoparticles (~ 5 nm) of Fe_3O_4/γ-Fe_2O_3. The partial reduction of Fe_3O_4 into γ-Fe_2O_3 also affects the M_S (25% of Fe_3O_4) in the nanoparticles. Also, the small particle size and crystallinity of nanoparticles leads to a lower magnetization value. The M_S of Fe_3O_4/γ-Fe_2O_3@$NaGdF_4$:Yb, Er was decreased due to the contribution of a low mass fraction of the $NaGdF_4$:Yb, Er with Fe_3O_4/γ-Fe_2O_3. Further, the M-H curve for Fe_3O_4/γ-Fe_2O_3@$NaGdF_4$:Ln^{3+} nanoparticles consists of two components, a superparamagnetic component with magnetic moment ~ 8 emu g^{-1}, and a paramagnetic component (linear slope at large applied fields). However, the overall M_s value of Fe_3O_4/γ-Fe_2O_3@$NaGdF_4$:Yb,Er showed satisfactory response to the external applied magnetic field (Inset, Figure 4).

The paramagnetic contributions in Fe_3O_4/γ-Fe_2O_3@$NaGdF_4$:Yb,Er and Ln^{3+}-doped $NaGdF_4$ nanocrystals featured mainly arising from Gd^{3+} ions. The seven unpaired electrons in the inner 4f subshells of the Gd^{3+} ions are tightly bound to the nucleus and shielded by the outer closed shell $5d^16s^2$ electrons from the crystal fields and are responsible for the magnetic characteristics of the Gd^{3+} ions. The magnetic moments related to the Gd^{3+} ions are all localized and non-interacting, which led to paramagnetism of the Gd^{3+} ions. Hence, under magnetic field the samples containing matrix of $NaGdF_4$ nanoparticles can induce relative magnetism and such samples recovers its initial state before applied field, when magnetic field is removed. This kind of effect is called magneto-optical interaction in $NaGdF_4$:Yb, Er nanoparticles and obtained under certain magnetic fields and the relative luminescence modulation may be accessible with a magnetic field. Generally, modulating luminescence of materials via magnetic fields needs the coupling of optical and magnetic interaction and it is believed that simultaneous realization of optical and magnetic properties in a single phase will avail optical and magnetic interaction within the crystal lattice and hence promising modulation luminescence via magnetic fields.[18]

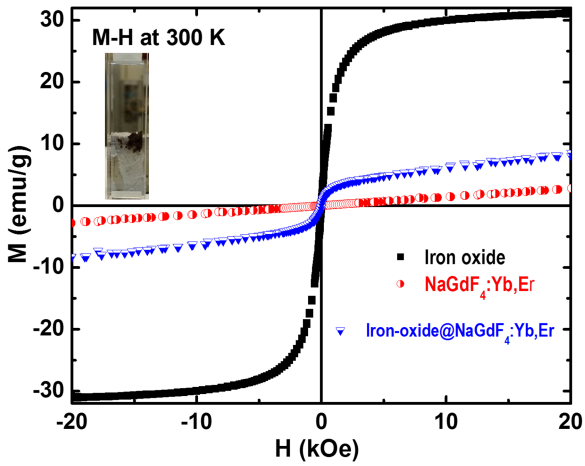

FIG. 4. Field dependent magnetization (M-H curves) of iron-oxide, paramagnetic $NaGdF_4$:Yb, Er, and magnetic luminescence Fe_3O_4/γ-Fe_2O_3@$NaGdF_4$:Yb,Er nanoparticles. Inset diagram shows that Fe_3O_4/γ-Fe_2O_3@$NaGdF_4$:Yb,Er nanoparticles attracted towards a bar magnet with sufficient magnetic characteristics for several applications.

CONCLUSION

To summarize, we have reported a microwave assisted solvothermal synthesis of multifunctional $NaGdF_4:Ln^{3+}$ and $Fe_3O_4/\gamma\text{-}Fe_2O_3@NaGdF_4:Ln^{3+}$ (Ln = Yb, Er) nanoparticles. This synthesis suggested morphological difference for both the samples as observed through XRD and HRTEM. The magnetic and luminescent properties of $Fe_3O_4/\gamma\text{-}Fe_2O_3@NaGdF_4:Ln^{3+}$ nanocomposites were compared with paramagnetic $NaGdF_4:Ln^{3+}$ and discussed in context to the possible luminescence quenching due to $Fe_3O_4/\gamma\text{-}Fe_2O_3$. The magnetic hysteresis at 300 K for $\beta\text{-}NaGdF_4:Ln^{3+}$ showed paramagnetic features; whereas $Fe_3O_4/\gamma\text{-}Fe_2O_3@\beta\text{-}NaGdF_4:Ln^{3+}$ exhibited superparamagnetic behavior with negligible coercive field. The luminescent properties with strong magnetic response in an external magnetic field and better stability of the nanocomposites can be used for the development of certain luminescence–magnetic composites for biomedical industry and may open up new opportunities in this field.

ACKNOWLEDGMENTS

This work was supported by the jointly CAPES, FAPEMA, and FAPEAL in Brazil and CONICET in Argentina.

[1] L. Sun, X. Ge, J. Liu, Y. Qiu, Z. Wei, B. Tian, and L. Shi, Nanoscale **6**, 13242 (2014).
[2] L. Zhang, W.-F. Dong, and H.-B. Sun, Nanoscale **5**, 7664 (2013).
[3] Y. R. Weng, J. Zhao, S. Y. Yu, and S. Y. Song, CrystEngComm **16**, 6257 (2014).
[4] C. Kaewsaneha, P. Tangboriboonrat, D. Polpanich, and A. Elaissari, ACS Appl. Mater. Interfaces **7**, 23373 (2015).
[5] C. Zhong, P. Yang, X. Li, C. Li, D. Wang, S. Gai, and J. Lin, RSC Adv. **2**, 3194 (2012).
[6] A. H. Lu, E. L. Salabas, and F. Schuth, Angew. Chemie - Int. Ed. **46**, 1222 (2007).
[7] H. Zhu, J. Tao, W. Wang, Y. Zhou, P. Li, Z. Li, K. Yan, S. Wu, K. W. K. Yeung, Z. Xu, H. Xu, and P. K. Chu, Biomaterials **34**, 2296 (2013).
[8] N. Shrivastava, L. U. Khan, Z. U. Khan, J. Vargas, O. Moscoso-Londoño, C. Ospina, H. F. Brito, Y. Javed, M. C. F. C. Felinto, A. S. de Menezes, M. Knobel, and S. K. Sharma, J. Mater. Chem. C 2282 (2017).
[9] Y.-S. Lin, S. Wu, Y. Hung, Y. Chou, C. Chang, M. Lin, C. Tsai, and C.-Y. Mou, Chem. Mater. **18**, 5170 (2006).
[10] M. N. Luwang, S. Chandra, D. Bahadur, and S. K. Srivastava, J. Mater. Chem. **22**, 3395 (2012).
[11] X. Zhang, Z. Zhao, X. Zhang, D. B. Cordes, B. Weeks, B. Qiu, K. Madanan, D. Sardar, and J. Chaudhuri, Nano Res. **8**, 636 (2015).
[12] J. Zhou, Q. Liu, W. Feng, Y. Sun, and F. Li, Chem. Rev. **115**, 395 (2015).
[13] N. Shrivastava, L. U. Khan, J. M. Vargas, C. Ospina, J. A. Q. Coaquira, G. Zoppellaro, H. F. Brito, Y. Javed, D. K. Shukla, M. C. F. C. Felinto, and S. K. Sharma, Phys. Chem. Chem. Phys. **19**, 18660 (2017).
[14] X. S. Ke, Y. Ning, J. Tang, J. Y. Hu, H. Y. Yin, G. X. Wang, Z. S. Yang, J. Jie, K. Liu, Z. S. Meng, Z. Zhang, H. Su, C. Shu, and J. L. Zhang, Chem. - A Eur. J. **22**, 9676 (2016).
[15] S. Sarveena, J. M. Vargas, D. K. Shukla, C. T. Meneses, P. Mendoza Zélis, M. Singh, and S. K. Sharma, Phys. Chem. Chem. Phys. **18**, 9561 (2016).
[16] G. Yi and G. Chow, Chem. Mater. **19**, 341 (2007).
[17] V. K. Pecharsky and P. Y. Zavalij, *B9-Fundamentals of Powder Diffraction and Structural Characterization of Materials* (2005).
[18] X. Zhang, Z. Zhao, X. Zhang, D. B. Cordes, B. Weeks, B. Qiu, K. Madanan, D. Sardar, and J. Chaudhuri, Nano Res. **8**, 636 (2015).